Corrosion Science 50 (2008) 2197–2204

Contents lists available at ScienceDirect

Corrosion Science

journal homepage: www.elsevier.com/locate/corsci

Kinetic modelling of the attenuation of carbon steel canister corrosion due to diffusive transport through corrosion product layers

J. Peña *, E. Torres, M.J. Turrero, A. Escribano, P.L. Martín

Engineered and Geological Barrier Unit, CIEMAT, Avda. Complutense, 22, 28040 Madrid, Spain

ARTICLE INFO

Article history:
Received 12 December 2007
Accepted 9 June 2008
Available online 17 June 2008

Keywords:
A. Iron
B. Modelling studies
C. Oxide coatings
C. Kinetic parameters

ABSTRACT

This work models the attenuation of the corrosion of carbon steel canisters due to the influence of diffusive transport through the corrosion product – a growing film of magnetite. The model makes use of an algorithm based on the analytical solution of 1D diffusion equations for the movement of Fe^{2+}, H_2, H_2O and OH^- through this magnetite film.

1. Introduction

Geological disposal is considered a safe solution to the management of high-level radioactive waste. The geological disposal of high-level radioactive waste is based in a multibarrier concept where radioactive wastes are surrounded consecutively by man-made barriers (which include the metallic canister and the bentonite barrier) and by natural barriers. As a result, the waste will be isolated from man and environment for a sufficiently long time such that an acceptable level of protection is ensured.

The main purpose of the metallic canister is to avoid the contact of water with the high-level radioactive waste. Carbon steel have been proposed in a number of deep geological repository concepts as a suitable corrosion allowance material for a canister. Their great merit is a low tendency to localized corrosion in a reducing repository environment. In most of possible repository conditions, carbon steel will corrode only by general corrosion.

The carbon steel canisters used for the geological disposal high-level radioactive waste can become corroded through interaction with pore water from the surrounding bentonite. Such corrosion can lead to their failure and the release of radionuclides to the bentonite barrier.

The corrosion of these canisters in the near field is assumed to be anaerobic [1]. Groundwater moves through the bentonite barrier, and, due to the efficient redox capacity of this mineral (a consequence of its sulphide [mainly pyrite] content), O_2-free groundwater comes into contact with the canisters [2,3]. Under these conditions, water is the most important oxidant [3] and magnetite the main corrosion product [4].

Magnetite films a have a polycrystalline structure [5–8]. The grain boundary diffusion coefficients of reactants and products moving through the corrosion film are between two and three orders of magnitude greater than the corresponding bulk diffusion coefficients [5,8]. Therefore grain boundary diffusion takes place rather than bulk diffusion [9–11].

The corrosion of iron by H_2O [12–18]has been proposed to involve two steps:

(1) The oxidation of iron and the precipitation of ferrous hydroxide with the generation of H_2:

$$Fe(s) + 2H_2O \Rightarrow Fe(OH)_2(s) + H_2 \quad (1)$$

(2) The transformation of ferrous hydroxide to magnetite at temperatures over 80 °C via the Schikorr reaction [19,20]:

$$3Fe(OH)_2(s) \rightarrow Fe_3O_4(s) + 2H_2O + H_2 \quad (2)$$

The overall reaction (combining Reactions (1) and (2)) is therefore:

$$3Fe(s) + 4H_2O \Rightarrow Fe_3O_4(s) + 4H_2 \quad (3)$$

Smart et al. [12,13] and Blackwood et al. [14] also suggest the participation of other reactions in the corrosion of iron by H_2O:

$$Fe(s) + 2H_2O \Rightarrow Fe^{2+} + H_2 + 2OH^- \quad (4)$$

and

$$3Fe^{2+} + 2OH^- + 2H_2O \Rightarrow Fe_3O_4 + 3H_2 \quad (5)$$

* Corresponding author. Tel.: +34 913460835; fax: +34 913466542.
E-mail address: javier.pena@ciemat.es (J. Peña).

0010-938X/$ - see front matter © 2008 Elsevier Ltd. All rights reserved.
doi:10.1016/j.corsci.2008.06.004

The rate-limiting step in the corrosion of carbon steel canisters used in radioactive waste storage is the diffusive transport of reactants and products through the corrosion product layers [5] [9] [10]. The thickness of the magnetite film influences the inward diffusion of oxidants and the outward diffusion of corrosion products, therefore, as it grows, the rate of corrosion should become attenuated. The aim of the present work was to model this attenuation along time. It has chosen a period of 16 years in the graphic representations because it has been observed that all attenuations happen within this period.

2. Modelling

The PHREEQC program [21] is a 1D-reactive transport code with an explicit finite difference algorithm for the calculation of 1D transport. This numerical approach follows the basic components of the advection–reaction–dispersion equation in a split-operator scheme. The advective transport of the transported solute is first calculated at each time step, followed by all equilibrium and kinetically controlled chemical reactions, then by its dispersive transport and its associated equilibrium and kinetically controlled chemical reactions [21].

PHREEQC has an embedded BASIC interpreter that allows the definition of rate expressions for kinetic reactions in the input file. These rate expressions can deal with a large number of chemical variables that the code calculates during execution. For example, at each time step a user employing the "KINETICS" keyword can determine the molar concentration of all equilibrium and kinetically controlled solid phase assemblages.

In the present work a rate expression for the kinetic reaction of iron corrosion by H_2O was programmed to run under PHREEQC. At each time step this expression was able to determine the amount of magnetite precipitated as a consequence of this corrosion. Assuming that magnetite precipitates uniformly over the corrosion surface, its molar quantity can be transformed into a thickness.

The kinetic treatment of dissolution or precipitation of a mineral phase in contact with water is described by an expression derived from transition state theory [22]. Simplifying the original expression the overall rate of mineral dissolution or precipitation is [21]:

$$r_+ = k_+(1 - \Omega^\sigma) \tag{6}$$

where r_+ is the specific rate (mol/m^2/s), k_+ is an empirical constant, and σ is a coefficient related to the stoichiometry of the reaction (this is often equal to 1 in dissolution reactions [23]), and Ω is the saturation ratio,

$$\Omega = \left(\frac{\mathrm{IAP}}{K}\right) \tag{7}$$

where IAP is the ionic activity product and K the equilibrium constant of the reaction. When the reaction approaches equilibrium (IAP/K = 1), the rate approaches zero.

In transport and reaction codes such as PHREEQC, speciation and equilibrium reactions are determined from a thermodynamic database based on the laws of mass action. These laws relate the formation of aqueous species, or the dissociation of mineral phases, with a series of reactants and products via equilibrium constants. In these calculations the reactants and products in the equations of the thermodynamic database may not necessarily be the same as those that actually take part in real reactions.

The thermodynamic database provided (llnl.dat [21]) the following reaction for metallic iron equilibrium:

$$\mathrm{Fe(s)} + 2\mathrm{H^+} + 0.5\mathrm{O_2} \Rightarrow \mathrm{Fe^{2+}} + \mathrm{H_2O} \tag{8}$$

The species involved in the corrosion of carbon steel by water are those that appear in Eq. (1)–(5). Eq. (4) includes all the aqueous species that participate in the process; therefore Eq. (8) was replaced by Eq. (4) (after recalculating the equilibrium constant). The ionic activity product of Eq. (4) is

$$\mathrm{IAP} = \{\mathrm{Fe^{2+}}\}\{\mathrm{H_2}\}\{\mathrm{OH^-}\}^2\{\mathrm{H_2O}\}^{-2} \tag{9}$$

Using Eq. (9), the PHREEQC program was used to calculate the saturation ratio Ω of iron with respect the bentonite pore water. When $0 > \Omega < 1$, corrosion would be possible, the rate of corrosion becoming smaller as Ω approximates to 1 (at which point corrosion stops). However, as a magnetite film builds up between the carbon steel and the bentonite pore water, is creating a new medium with new transport properties. The code PHREEQC can not create this new medium during the simulation. To solve this problem, it is estimated (through analytical solutions of diffusive transport equations), which would be the concentration of the species involved in the corrosion of iron in this new medium, and calculates a new IAP. All this is included in the equation kinetic corrosion of iron which applies at one end of the system modelled composed entirely of bentonite. This equation is formed by a constant speed and an expression that takes into account the equilibrium, modified for the new IAP.

The approximation followed consisted in analytically resolving at each time step the diffusive transport occurring through the magnetite film - both that of the reactants moving towards the carbon steel and that of the products moving towards the bentonite.

Analytical solutions are usually used to validate numerical solutions in simple situations, e.g., in finite columns where $C_{\infty,t} = 0$ [21,24]. They have also been used in the study of diffusion across the grain boundary of thin films [11,25]. In the present work both analytical and numerical approximations were used, depending on their applicability.

The analytical solution of 1D diffusive transport when considering an infinite column in which $C_{x,0} = 0$, $C_{0,t} = C_0$, and $C_{\infty,t} = 0$, is [21]:

$$C_{x,t} = C_0 \mathrm{erfc}\left(\frac{x}{\sqrt{4D_e t}}\right) \tag{10}$$

where D_e is the effective diffusion coefficient.

The analytical solution of a diffusion case with a constant source and a diffusion barrier grain boundary dominated such as a finite thickness films, is [11]:

$$C_{L_F,t} = C_0 + 4\frac{C_0}{\pi}\sum_{n=0}^{\infty}\frac{(-1)^{n+1}}{2n+1}\exp\left[-\frac{D_{GB}t(2n+1)^2\pi^2}{4L_F^2}\right] \tag{11}$$

where C_0 is the concentration at the source point, L_F is the thickness of the film, and D_{GB} is the effective diffusion coefficient when diffusion will take place only in the space available at the grain boundary. This is best solved when $n = 5$ [25].

To apply this to the simulation of carbon steel canister corrosion, a 1D system was defined consistent with the set of cells formed by the bentonite, the boundaries of which coincide on

Table 1
Inicial chemistry of the pore water of bentonite used in this study (from [26])

pH	7.44
Na (M)	3.9×10^{-1}
K (M)	3.0×10^{-3}
Mg (M)	9.7×10^{-2}
Ca (M)	8.2×10^{-2}
Cl (M)	7.3×10^{-1}
SO_4 (M)	1.7×10^{-2}
$C_{inorg.}$ (M)	2.4×10^{-4}
Si (M)	1.8×10^{-4}

one side with the container/bentonite interface and on the other with that of the bentonite and the geological medium. These boundaries are defined by environmental conditions. The conditions used in the present modelling procedure were Neumann or no-flux conditions reigned at both boundaries. At time zero bentonite water filled the bentonite pores, the chemical composition of which was obtained from Fernández et al. [26]. This chemical composition is showed in Table 1. This water was equilibrated during all the simulation time with an ion exchanger composed of NaX, KX, CaX_2, MgX_2, FeX_2, FeClX and CaClX. The selectivity coefficients for FeClX and CaClX, were described by Charlet and Tournassat [27]. See Table 2 for values of selectivity coefficients. This water was equilibrated with a phase mineral assemblage for a specific amount [26] of calcite, gypsum, chalcedony and halite. This mineral assemblage also includes those not existing at the beginning but along the simulation might form and dissolve. Look at Table 3 for values of this mineral assemblage. Thermodynamic constants for green rust minerals were described by Bourrie et al., [28].

The system was spatially divided over 20 cells of length 0.025 m (total length 0.5 m). Cell 1 had a constant temperature of 25 °C and represented bentonite close to the bentonite/concrete boundary. Cell 20 had a constant temperature of 100 °C and represented bentonite close to the bentonite/canister boundary (Fig. 1). The film of magnetite consisted of grains and grain boundaries. In order to model this film, a reaction zone or sink and accumulation region [11,25] of thickness γ was required, where the new saturation ratio with respect to iron was calculated (Fig. 1).

Eq. (11) was used to calculate the activity of the H_2O that crossed the magnetite of thickness L_F:

$$[H_2O]_S = [H_2O]_{20} + 4\frac{[H_2O]_{20}}{\pi}\sum_{n=0}^{\infty}\frac{(-1)^{n+1}}{2n+1}\exp\left[-\frac{D_{H_2O}t(2n+1)^2\pi^2}{4L_F^2}\right] \quad (12)$$

$$\{H_2O\}_S = [H_2O]_S\gamma_{H_2O} \quad (12b)$$

where $\{H_2O\}_S$ is the activity of the water in the sink and accumulation region, γ_{H_2O} is the activity coefficient for H_2O, $[H_2O]_S$ the molality of the H_2O in the sink and accumulation region, $[H_2O]_{20}$ the molality of H_2O in cell 20, D_{H_2O} the effective diffusion coefficient for H_2O at the grain boundary of the magnetite film, and t the simulation time.

Somewhat more difficult is the determination of the activity of the reaction products of Eq. (4) in the water that occupies the reaction zone (sink and accumulation region) based on the concentration results for cell 20 (see Fig. 1) provided by the PHREEQC program. In this work, and at each time step, the mass balance was established between the mass of the reaction products in the cell in contact with the metallic iron, and the mass of these products in the reaction zone thought to exist between the carbon steel and the magnetite film, plus that in the water at the magnetite grain boundary (should it exist), plus that in the water between the bentonite cell and the metallic iron (should there be a magnetite film). This mass balance can be described as follows (Fig. 2):

$$C_{20}V_{20} = \overline{C}_S V_S + \overline{C}_{GB}V_{GB} + \overline{C}^*_{20}V_{20} \quad (13)$$

where C_{20} is the concentration of cell 20 (the cell in contact with the metallic iron), V_{20} is the volume occupied by the pore water in this cell, C_S the concentration of the reaction products in the water of the reaction zone, V_S the volume of this zone, C_{GB} the concentration of the water in the grain boundary of the forming magnetite, V_{GB} the volume occupied by the grain boundary, and C^*_{20} the concentration of the reaction products in cell 20 remaining in the magnetite.

If we assume that the reaction zone is a high diffusivity region, then:

$$\overline{C}_S = C_S^{x=\gamma} \quad (14)$$

If the mean concentration of the reaction products in the region of the grain boundary, $\overline{C}_{GB}$, is equal to their mean concentration (see Fig. 2) at the boundary of the accumulation zone and the limit of the bentonite boundary,

$$\overline{C}_{GB} = \frac{C_{GB}^{x=\gamma} + C_{GB}^{x=\gamma+L}}{2} \quad (15)$$

then the concentration of the reaction products at the magnetite/bentonite boundary can be calculated using Eq. (11). Since the reaction zone is a high diffusivity region, then the expression

$$C_{GB}^{x=\gamma} = \overline{C}_S \quad (16)$$

represents the initial concentration of the reaction products, C_0, in Eq. (11):

$$C_{GB}^{x=\gamma+L} = \overline{C}_S + 4\frac{\overline{C}_S}{\pi}\sum_{n=0}^{\infty}\frac{(-1)^{n+1}}{2n+1}\exp\left[-\frac{D_{GB}t(2n+1)^2\pi^2}{4L_F^2}\right] \quad (17)$$

Table 2
Selectivity coefficients (K_C) for exchange reactions for bentonita according to Gaines–Thomas convection

Exchange reaction	K_C	References
$NaX + K^+ \leftrightarrow KX + Na^+$	10.6	[26]
$2NaX + Ca^{2+} \leftrightarrow CaX_2 + 2Na^+$	12.8	[26]
$2NaX + Mg^{2+} \leftrightarrow MgX_2 + 2Na^+$	10.7	[26]
$NaX + CaCl^+ \leftrightarrow CaClX + Na^+$	316.2	[27]
$2NaX + Fe^{2+} \leftrightarrow FeX_2 + 2Na^+$	2.75	[21]
$NaX + FeCl^+ \leftrightarrow FeClX + Na^+$	199.5	[27]

Table 3
Chemical values of mineral assemblage

Mineral	Formula	Log K	Initial content (wt.%) [26]	References
Calcite	$CaCO_3 + H^+ = Ca^{2+} + HCO_3^-$	1.85	0.6	[21] llnl.dat
Dolomite(dis)	$CaMg(CO_3)_2 + 2H^+ = Ca^{2+} + Mg^{2+} + 2HCO_3^-$	4.06		[21] llnl.dat
Gypsum	$CaSO_4 : 2H_2O = Ca^{2+} + SO_4^{2-} + 2H_2O$	−4.48	0.14	[21] llnl.dat
Chalcedony	$SiO_2(s) = SiO_{2+}(aq)$	−3.73	2.0	[21] llnl.dat
Halite	$NaCl = Na^+ + Cl^-$	1.59	0.13	[21] llnl.dat
Magnetite	$Fe_3O_4 + 8H^+ = Fe^{2+} + 2Fe^{3+} + 4H_2O$	10.47		[21] llnl.dat
Fe(OH)2	$Fe(OH)_2 + 2H^+ = Fe^{2+} + 2H_2O$	13.90		[21] llnl.dat
Goethite	$FeOOH + 3H^+ = Fe^{3+} + 2H_2O$	0.53		[21] llnl.dat
Lepidocrocite	$FeOOH + 3H^+ = Fe^{3+} + 2H_2O$	1.37		[21] minteq.dat
Siderite	$FeCO_3 + H^+ = Fe^{2+} + HCO_3^-$	-0.19		[21] llnl.dat
Greenrust-Cl	$Fe_4(OH)_8Cl + 8H^+ = 3Fe^{2+} + Fe^{3+} + Cl^- + 8H_2O$	21.92		[28]
Greenrust-SO_4	$Fe_6(OH)_{12}SO_4 + 12H^+ = 4Fe^{2+} + 2Fe^{3+} + SO_4^{2-} + 12H_2O$	22.88		[28]
Greenrust-CO_3	$Fe_6(OH)_{12}CO_3 + 12H^+ = 4Fe^{2+} + 2Fe^{3+} + CO_3^{2-} + 12H_2O$	19.42		[28]

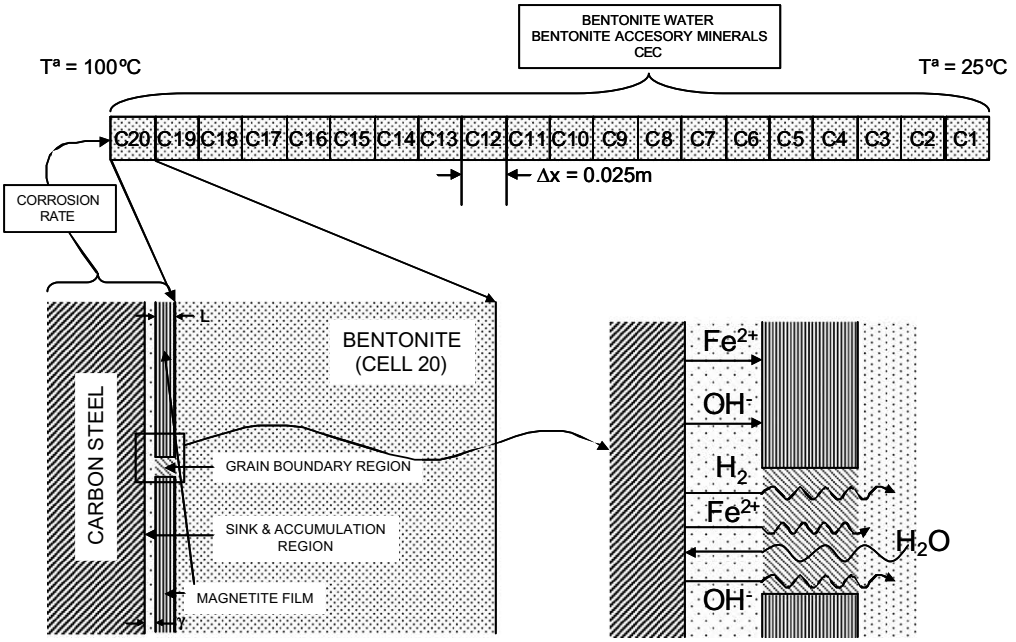

Fig. 1. Model of the near field system.

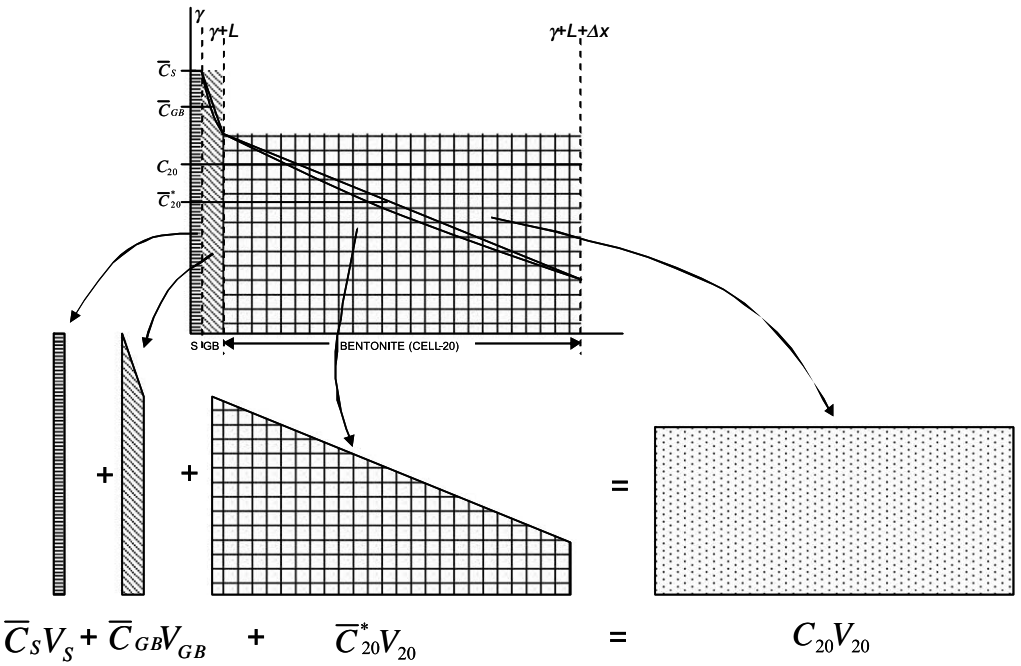

Fig. 2. Graphical representation of the mass balance equation (13).

Introducing Eqs. (16) and (17) into Eq. (15) provides the expression:

$$\overline{C}_{GB} = \frac{\overline{C}_S + \left\{\overline{C}_S + 4\frac{\overline{C}_S}{\pi}\sum_{n=0}^{\infty}\frac{(-1)^{n+1}}{2n+1}\exp\left[-\frac{D_{GB}t(2n+1)^2\pi^2}{4L_F^2}\right]\right\}}{2} \tag{18}$$

In the same way as Eq. (15), Eq. (19) provides the mean concentration of the reaction products that ought to be found in cell 20:

$$\overline{C}^*_{20} = \frac{C^{*x=\gamma+L}_{20} + C^{*x=\gamma+L+\Delta x}_{20}}{2} \tag{19}$$

where $C^{*x=\gamma+L}_{20}$ is the concentration of the reaction products at the boundary between the magnetite film and the bentonite of cell 20, and $C^{*x=\gamma+L+\Delta x}_{20}$ that of the reaction products at the interface between cell 20 and cell 19. The concentration of the reaction products at the boundary between the magnetite and cell 20 is

$$C^{*x=\gamma+L}_{20} = C^{x=\gamma+L}_{GB} \tag{20}$$

Eqs. (10) and (20) can then be used to calculate the concentration of the reaction products at the opposite extreme of cell 20 (i.e., where it meets cell 19) to provide:

$$C_{20}^{*x=\gamma+L+\Delta x} = C_{GB}^{x=\gamma+L}\mathrm{erfc}\left(\frac{\Delta x}{\sqrt{4D_{20}t}}\right) \quad (21)$$

Introducing Eqs. (17), (20), and (21) into (19) provides the expression:

$$\overline{C}_{20}^{*} = \frac{\overline{C}_S}{2}\left(\left\{1+\frac{4}{\pi}\sum \mathrm{GB}\right\} + \left\{\left(1+\frac{4}{\pi}\sum \mathrm{GB})\mathrm{erfc}(20)\right)\right\}\right) \quad (22)$$

where

$$\sum \mathrm{GB} = \sum_{n=0}^{\infty}\frac{(-1)^{n+1}}{2n+1}\exp\left[-\frac{D_{GB}t(2n+1)^2\pi^2}{4L_F^2}\right] \quad (23)$$

and

$$\mathrm{erfc}(20) = \mathrm{erfc}\left(\frac{\Delta x}{\sqrt{4D_{20}t}}\right) \quad (24)$$

Introducing Eqs. (18) and (22) into (13), and making use of Eqs. (23) and (24), provides the expression:

$$\overline{C}_{20}V_{20} = \overline{C}_S V_S + \overline{C}_S(2+\frac{4}{\pi}\sum \mathrm{GB})\frac{V_{GB}}{2} + \overline{C}_S\left(\left\{1+\frac{4}{\pi}\sum \mathrm{GB}\right\} + \left\{\left(1+\frac{4}{\pi}\sum GB\right)\mathrm{erfc}(20)\right\}\right)\frac{V_{20}}{2} \quad (25)$$

The main point of interest is the concentration of the reaction products $\overline{C}_S$ in the reaction zone. To determine this, (24) can be rewritten to provide the following:

$$\overline{C}_S = \overline{C}_{20}\frac{V_{20}}{V_S + (2+\frac{4}{\pi}\sum \mathrm{GB})\frac{V_{GB}}{2} + (\{1+\frac{4}{\pi}\sum \mathrm{GB}\} + \{(1+\frac{4}{\pi}\sum \mathrm{GB})\mathrm{erfc}(20)\})\frac{V_{20}}{2}} \quad (26)$$

Finally, the activity of the reaction products, $\overline{A}_S$, is determined by multiplying $\overline{C}_S$ by the activity coefficient γ:

$$\overline{A}_S = \overline{C}_S\gamma \quad (26b)$$

This equation can then be used to calculate the activity of the reaction products in the reaction zone. These, plus the activity of the water, determined using Eq. (12b), allow the recalculation of the ionic activity product (IAP_S) in the reaction zone:

$$IAP_S = \{Fe^{2+}\}_S\{H_2\}_S\{OH^-\}_S^2\{H_2O\}_S^{-2} \quad (27)$$

Thus, the new corrosion rate for the carbon steel would be:

$$R_+ = k_+\left(1-\frac{IAP_S}{K}\right) \quad (28)$$

The value of V_{GB} can then be calculated from the thickness of the magnetite film (L), the surface area occupied by this film (A), and the fraction of the cross sectional area occupied by the grain boundary ϕ:

$$V_F = L\times A\times\phi \quad (29)$$

The grain boundary of the magnetite film occupies up to 5–8% of the in-plane cross-sectional area of the film itself [5] (in the present work a value of $\phi = 0.05$ [i.e., 5%] was used).

3. Results

Fig. 3 shows the changing corrosion rate over 16 years of modelling with different grain boundary diffusion coefficients. Results for diffusion without attenuation are also provided for comparison. Table 4 shows the sets of effective diffusion coefficients through the magnetite film for all the reactants and reaction products taken into account. All the corrosion rate values showed reductions from the initial rate (25 m/y). The magnitude and rate of these reductions depend on the set of effective diffusion coefficients used.

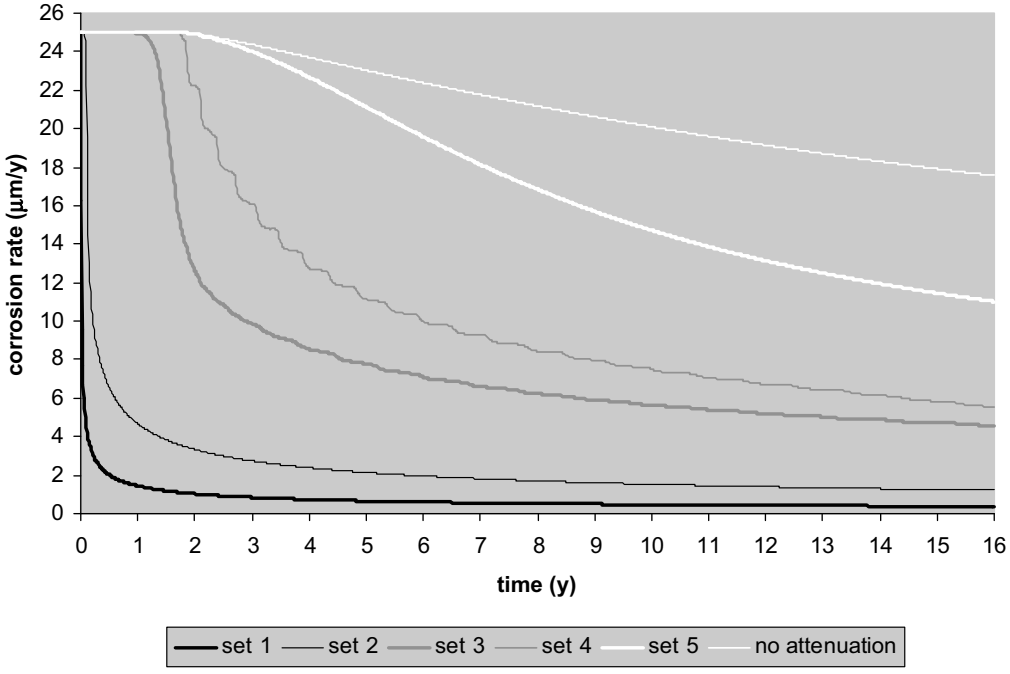

Fig. 3. Attenuation of corrosion rate over 16 years for different sets of effective diffusion coefficients.

Table 4
Effective diffusion coefficients used in simulations

	D_{H_2O}, H_2, OH^- (m^2/s)	D_{Fe2+} (m^2/s)
Set 1	10^{-19}	10^{-20}
Set 2	10^{-18}	10^{-19}
Set 3	10^{-17}	10^{-18}
Set 4	10^{-16}	10^{-17}
Set 5	10^{-15}	10^{-16}

For lower values, greater and faster attenuations of corrosion are seen. Simulation without attenuation only showed a small reduction in the corrosion rate due to the accumulation of the corrosion product on the bentonite in cell 20, but not in the sink and attenuation region as seen in simulations involving the proposed model.

Fig. 4 shows the depth of corrosion associated with the corrosion rates in Fig. 3. At the end of the simulation period these depths ranged from 11 m for parameter set 1 to 275 μm for parameter

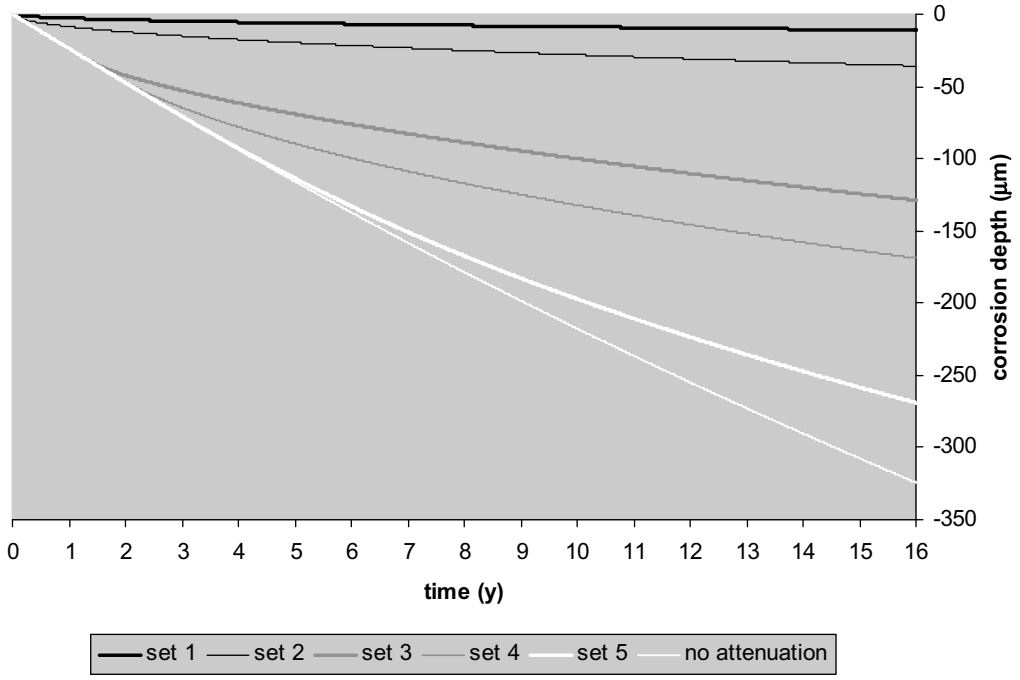

Fig. 4. Corrosion depth over 16 years for different sets of effective diffusion coefficients.

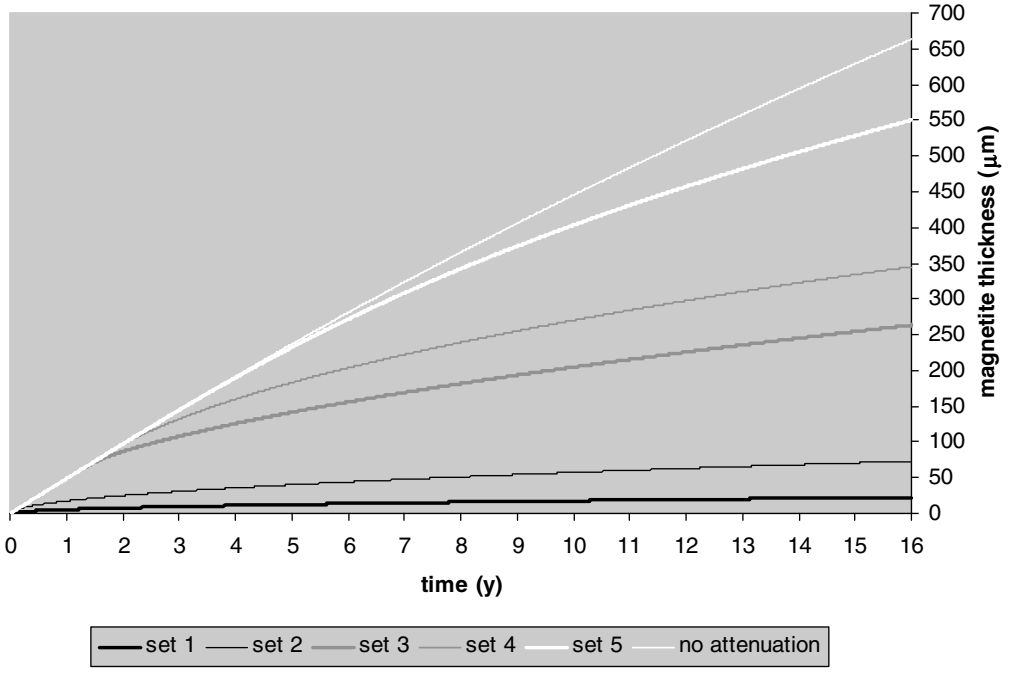

Fig. 5. Thickness of magnetite over 16 years for different sets of effective diffusion coefficients.

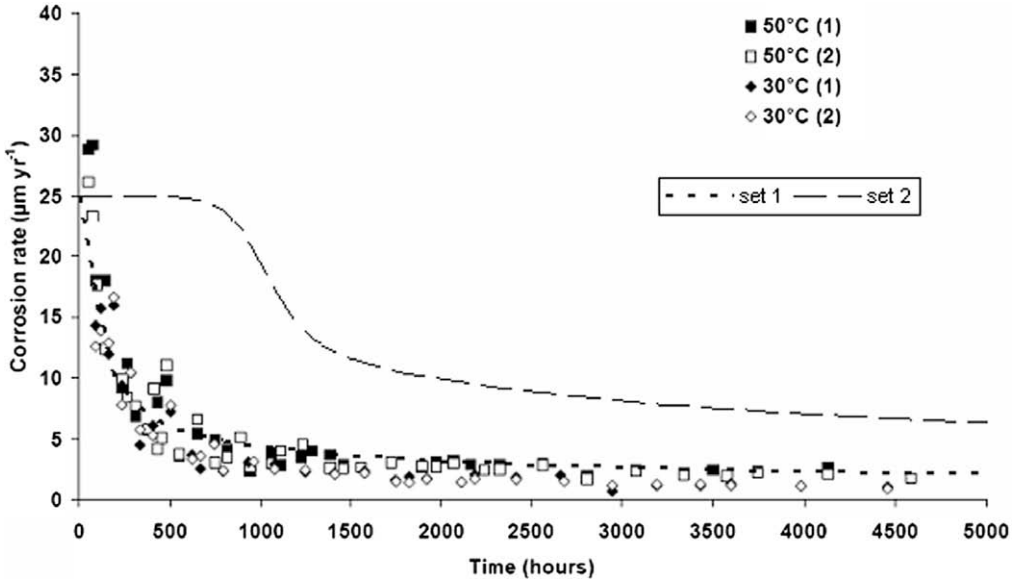

Fig. 6. Anaerobic corrosion rates for steel in compacted bentonite at pH 8.4 in a 1 M chloride solution at 30 °C and 50 °C. Reproduced from [29]. Also corrosion rate from present work simulated with parameter set 1 and 2.

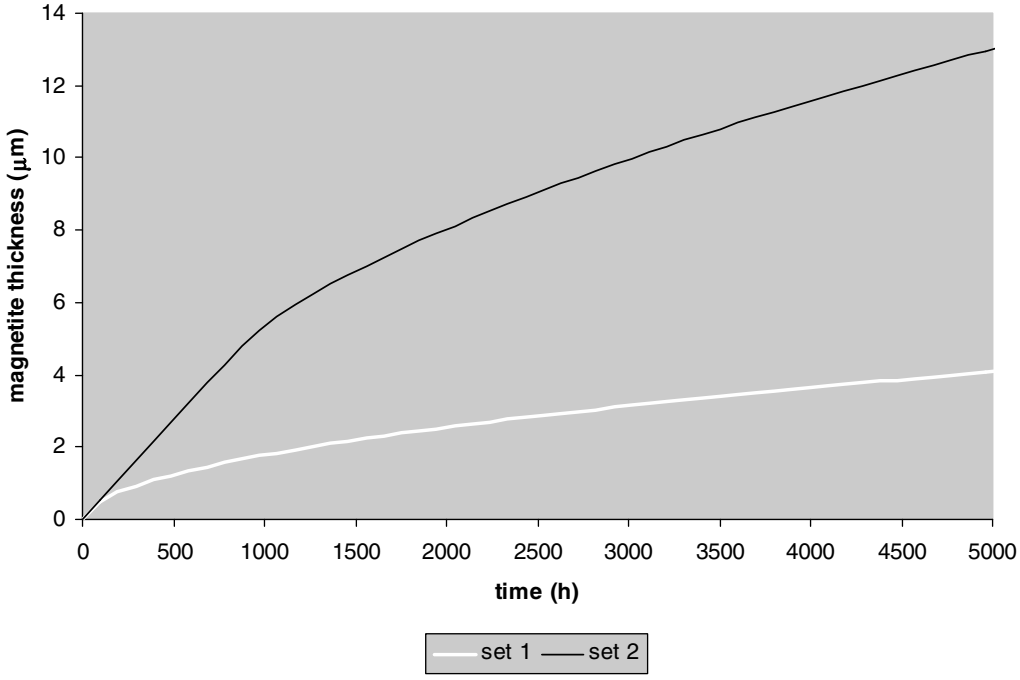

Fig. 7. Evolution of the thickness of the magnetite film simulated with parameter set 1 and 2.

set 5. When no diffusion attenuation was included, a final corrosion depth of 325 μm was seen.

Fig. 5 shows the magnetite film thickness associated with the rates of corrosion in Fig. 2. At the end of simulation time these ranged from 22 μm for set 1 to 550 μm for set 5. When no diffusion attenuation was included, a final magnetite film thickness of 650 μm was seen.

4. Discussion

Smart et al. [29] studied the corrosion rate of steel in bentonite under a wide range of conditions. Corrosion rates were measured by collecting the hydrogen produced. Fig. 6 shows this corrosion rate and also the results of the present work over a similar time scale using parameter sets 1 and 2. Fig. 7 shows the thickness of the magnetite over the same period, for cases 1 and 2.

The attenuation model reproduced the experimentally measured data of the above authors very well when parameter set 1 was used. This suggests that the magnitudes of the "set 1" parameters are near to real values. With respect to Fe^{2+}, the corrosion seen when using parameter set 1 did not differ much from the value of the grain boundary cation diffusion through magnetite calculated by Hendy et al. [5] ($D_{GB} = 2 \times 10^{-19}$ m^2/s compared to the present 10^{-20} m^2/s).

In Figs. 3 and 6, one can observe a platform of increasing amplitude to higher rates of diffusion, where the rate of corrosion is not decreasing. In the simulation number 1 was not appreciated because it happens within the first time step. Fig. 7 shows that the magnetite is formed since the beginning of the simulation, but for each diffusion coefficient used seems that there is a threshold thickness of magnetite from which the speed of corrosion begins to decline faster.

5. Conclusions

This paper reports a 1D diffusion attenuation model for the corrosion of carbon steel canisters, which simulates the reduction in the corrosion rate due to the formation of a magnetite film. The model was introduced into the PHREEQC program. The mass balance between three zones, the bentonite cell in contact with the canister, the accumulation region and the grain boundary region, allowed the activity of the chemical species involved in the corrosion of the iron canister by H_2O to be recalculated. From these new activities, the IAP of iron corrosion reaction is recalculated and incorporated into the expression of iron corrosion used in this work. The evaluation of this expression show a progressive reduction of the corrosion rate as the effective diffusion coefficients are reduced. The corrosion rates experimentally observed by others are well reproduced by the present model when set 1 of parameters are used. It has been observed a threshold thickness of magnetite from which the speed of corrosion begins to decline faster.

Acknowledgments

This is a contribution to the NF-Pro IP number FIGW-CT-2003-02389 financed by the EU and the CIEMAT/ENRESA association.

References

[1] P. Wersin, K. Spahiu, J. Bruno, Time evolution of dissolved oxygen and redox conditions in a HLW repository, SKB TR-94-02 1994.
[2] J. Bruno, D. Arcos, L. Duro, Processes and features affecting the near field hydrochemistry, Groundwater-bentonite interaction, SKB-TR-99-29, 1999.
[3] D. Arcos, J. Bruno, L. Duro, M. Grivé, Desarrollo de un modelo geoquímico de campo próximo, Publicación Técnica de ENRESA (2000). 4/2000.
[4] W. Stumm, J.J. Morgan, Aquatic Chemistry, Chemical Equilibria and Rates in Natural Waters, John Wiley & Sons, Inc., New York, 1996.
[5] S.C. Hendy, N.J. Laycock, M.P. Ryan, Atomistic modelling of cation transport in the passive film on iron and implications for models of growth kinetics, Journal of the Electrochemical Society 152 (8) (2005) B271–B276.
[6] M.F. Toney, A.J. Davenport, L.J. Oblonsky, M.P. Ryan, C.M. Vitus, Atomic structure of the passive oxide film formed on iron, Physical Review Letters 79 (1997) 21.
[7] V. Chevrier, P.E. Mathé, P. Rochette, O. Grauby, G. Bourrié, F. Trolard, Iron weathering products in a CO_2 + (H_2O or H_2O_2) atmosphere: Implications for weathering processes on the surface of Mars, Geochimica et Cosmochimica Acta 70 (2006) 4295–4317.
[8] V.B. Trindade, U. Krupp, H.J. Christ, Modelling of internal oxidation/corrosion, in: OPTICORR Guide Book, Optimisation of in service performance of boiler steels by modelling high temperature corrosion, EUR 21736 EN 2005.
[9] C. Desgranges, N. Bertrand, D. Gauvain, A. Terlain, D. Poquillon, D. Monceau, Model for low temperature oxidation during long-term. Prediction of Long Term Corrosion Behaviour in Nuclear Waste Systems, in: Proceedings of the Second International Workshop, Nice, September 2004, pp. 170–179.
[10] J. Robertson, The mechanism of high temperature aqueous corrosion of stainless steels, Corrosion Science 32 (1991) 4.
[11] M. DiBattista, J.W. Schwank, Determination of diffusion in polycrystalline platinum thin films, Journal of Applied Physics 86 (1999) 9.
[12] N.R. Smart, D.J. Blackwood, L. Werme, Anaerobic corrosion of carbon steel and cast iron in artificial groundwaters: part 1 – electrochemical aspects, Corrosion 58 (7) (2002) 547–559.
[13] N.R. Smart, D.J. Blackwood, L. Werme, Anaerobic corrosion of carbon steel and cast iron in artificial groundwaters: part 2-gas generation, Corrosion 58 (8) (2002) 627–637.
[14] D.J. Blackwood, A.R. Hoch, C.C, Naish, A.A. Rance, S.M. Sharland, Research on corrosion aspects of Advanced Cold Process Canister, SKB TR 94-12, 1994.
[15] D.J. Blackwood, C.C. Naish, The effect of galvanic coupling between the copper outer canister and the carbon steel inner canister on the corrosion resistance of the advanced cold Process Canister, SKB PR 95-04, 1995.
[16] D.J. Blackwood, C.C. Naish, N. Platts, K.J. Taylor, M.I. Thomas, The anaerobic corrosion of carbon iron in granitic groundwaters, SKB TR 95-03, 1995.
[17] N. Platts, D.J. Blackwood, C.C. Naish. Anaerobic oxidation of carbon iron in granitic groundwaters: A review of the relevant literature, SKB TR 94-01, 1994.
[18] N. Smart, A. Rance, D. Blackwood, Corrosion aspects of the copper-steel/iron process canister: Consequence of changing the material for the inner container from carbon steel to cast iron, SKB PR 97-04 1997.
[19] E.J. Reardon, Anaerobic corrosion of granular iron: Measurement and interpretation of hydrogen evolution rates, Environmental Science and Technology 29 (1995) 2936–2945.
[20] G.Z. Schikorr, Uber die reaktionen zwischen eisen, seinen hydroxyden und wasser, Elektrochimica 35 (1929) 62–65.
[21] D.L. Parkhust, C.A.J. Appelo, User's guide to PHREEQC (Version 2)- A computer program for speciation, reaction-path, 1D-Transport and inverse geochemical calculations, Report 99-4259, US Geological Survey, Water Resources Investigations, 1999.
[22] P. Aagaard, H.C. Helgeson, Thermodynamic and kinetic constraints on reaction rates among minerals and aqueous solutions; I, Theoretical considerations, American Journal of Science 282 (1982) 237.
[23] C.I. Steefel, P. Van Cappellen, A new kinetic approach to modelling water-rock interaction: The role of nucleation, precursors, and Ostwald ripening, Geochimica et Cosmochimica Acta 54 (1990) 2657–2677.
[24] C.A.J. Appelo, D. Postma, Geochemistry, Groundwater and Pollution, Rotterdam: Brookfield, 1996.
[25] P.H. Holloway, G.E. McGuire, Analysis of grain boundary permeation in solids, Journal of Electrochemistry and Society 125 (1978) 2070.
[26] A.M. Fernández, B. Baeyens, M. Bradbury, P. Rivas, Analysis of the porewater chemical composition of a Spanish compacted bentonite used in an engineered barrier, Physics and Chemistry of the Earth 29 (2004) 105–118.
[27] L. Charlet, C. Tournassat, Fe(II)–Na(I)–Ca(II) cation exchange on montmorillonite in chloride medium: evidence for preferential clay adsorption of chloride– metal ion pairs in seawater, Aquatic Geochemistry 11 (2) (2005) 115–137. June, (23) 2005.
[28] G. Bourrié, F. Trolard, J. Génin, A. Jaffrezic, V. Maître, M. Abdelmoula, Iron control by equilibria between hydroxy-green rusts and solutions in hydromorphic soils, Geochimica Cosmochimica Acta 63 (19-20) (1999) 3417–3427.
[29] N. Smart, A.P. Rance, L. Carlson, L.O. Werme, Further Studies of the Anaerobic Corrosion of Steel in Bentonite, in: P.V. Isheghem, (Ed.), Scientific Basis for Nuclear Waste Management XXIX, 2006.